Ferroelastic phase transition in $K_3Na(CrO_4)_2$ single crystals: an electron paramagnetic resonance study

2003 J. Phys.: Condens. Matter 15 8725

(http://iopscience.iop.org/0953-8984/15/50/007)

INSTITUTE OF PHYSICS PUBLISHING JOURNAL OF PHYSICS: CONDENSED MATTER

J. Phys.: Condens. Matter **15** (2003) 8725–8736 PII: S0953-8984(03)68356-6

Ferroelastic phase transition in $K_3Na(CrO_4)_2$ single crystals: an electron paramagnetic resonance study

S Jerzak

Department of Physics and Astronomy, York University, 4700 Keele Street, Toronto, M3J 1P3, Canada

Received 3 September 2003
Published 3 December 2003
Online at stacks.iop.org/JPhysCM/15/8725

Abstract

The phase transition in $K_3Na(CrO_4)_2$ single crystals has been studied by electron paramagnetic resonance (EPR) of Mn^{2+} ions. The values of the spin-Hamiltonian parameters have been evaluated. Below the phase transition temperature, the magnetic z-axis is deflected in *ac* and *bc* crystallographic planes by the same angle. Anomalous line shapes recorded below the phase transition temperature suggest the existence of an incommensurate phase.

1. Introduction

Interest in $K_3Na(CrO_4)_2$ (KNCr, hereafter) stems primarily from the unusual transformation of this material into a ferroelastic state. The temperature of this transformation is controversial and is reported to be 239 K [1] and 231 K [2]. The phase transition is classified as an improper one as evidenced by the doubling of the unit cell in the ferroelastic phase [3]. Three ferroelastic domains with 120° orientations were observed and switched by application of stress [1]. Elastic properties using the torsion pendulum technique show that the transition is driven by two-component order parameters related to the shear moduli c_{44} and c_{66} [1].

KNCr is isostructural with three other crystals of the general formula $K_3Na(XO_4)_2$, where X = S, Se, Cr, Mo (glaserite subfamily of crystals). $K_3Na(MoO_4)_2$ is ferroelastic below 513 K [4] and $K_3Na(SeO_4)_2$ (KNSe) below 334 K [5, 6]. Ferroelasticity in $K_3Na(SO_4)_2$ has not been observed.

The order of the phase transitions (first versus second) is unclear. According to dielectric, thermal and elastic studies, the phase transition was deduced to be of second-order (continuous) type. However, a small entropy change detected at the phase transition using DTA (differential thermal analysis), symmetry considerations and an abrupt change of frequency of modes observed in Brillouin scattering studies [1, 2], point to a weak first-order phase transition, although no temperature hysteresis has been detected so far at the phase transition.

The molecular mechanism of the phase transition is not fully understood. X-ray diffraction conducted at 291 and 200 K shows that the crystal symmetry changes from $P\bar{3}m1$ to $C2/c$ [3]. The phase transition is accompanied by shifts of K^+ ions. Two non-equivalent potassium ions,

0953-8984/03/508725+12$30.00

designated K(1) and K(2), are coordinated by 10 and 12 oxygens respectively. The K(1)–O(1) bond is particularly short. The cation bond valence sum for K(1) is 1.16, while it is only 0.91 for K(2) and 1.32 for Na. Potassium at the K(2) site is the most weakly bound cation in the structure. It has been suggested that the under-bonding of K(2) might lead to instability of the crystal structure [3].

The distribution of Cr–O bonds is similar to those in KNSe and KNS crystals: the bond Cr–O(1) is particularly short, indicating librational movement. It was found that CrO_4^{2-} anions shift and tilt at the phase transition. The deviation of the Cr–O(1) bond from the three-fold symmetry axis is about 7° at 200 K [3].

Two different models of the thermodynamic potential energy have been proposed to account for anomalies of various quantities occurring at the phase transition. One of the models [5] includes third-order degree terms of the order parameter. This model suggests the existence of a metastable phase in the crystal and accounts for the weak first-order character of the phase transition. The other model, originally constructed for the KNSe crystal, was suggested to be valid for KNCr as well [6]. A two-dimensional irreducible representation $A_3^+(q_1, 0)$ induces the phase transition from $P\overline{3}m1$ to $B2/m$, leading to the doubling of the unit cell. In the KNSe crystal this phase transition occurs at 346 K. At 329 K, the order parameter jumps from $(q_1, 0)$ to $(0, q_2)$ and the irreducible representation $A_3^+(0, q_2)$ leads to a space group change from $B2/m$ to $C2/c$. This model explains the existence of an intermediate phase in the KNSe crystal. An intermediate phase has not been observed in the KNCr crystal.

2. Experimental procedure

Single crystals of KNCr were grown isothermally from a saturated aqueous solution of Na_2CrO_4 and K_2CrO_4 mixed in stoichiometric proportion. Three types of crystal were grown: pure, doped with Mn^{2+} ions and doped with SeO_4^{2-} anions. Crystals grew in the form of hexagonal plates, yellow-orange in colour. The un-twinned portion of the crystal was taken for EPR measurements. Pure crystals were gamma irradiated (^{60}Co source, dose 1.1×10^6 rad) in order to create CrO_4^{3-} radicals. Unfortunately, the radicals decayed very quickly and no EPR spectra could be recorded. Irradiation of crystals doped with SeO_4^{2-} anions creates various radicals. All radicals detected were due to isotopes with the nuclear spin $I = 0$. Unfortunately, SeO_3^- or SeO_4^{3-} radicals with well separated hyperfine doublets due to the isotope ^{77}Se (nuclear spin $I = 1/2$, abundance 7.58%), which were successfully used to study the KNSe crystal [7], could not be observed despite the high irradiation dose. The EPR spectra were recorded on a Bruker X-band spectrometer. The sample temperature was changed by gently blowing nitrogen gas passing through the temperature controller.

3. Experimental results and discussion

The EPR spectrum (first derivative) of Mn^{2+}-doped KNCr crystal for the magnetic field parallel to the crystallographic a and c axes is shown in figures 1(a) and (b) respectively. The spectrum consists of five sextets and is typical for the Mn^{2+} ion, with electronic spin $S = 5/2$ and nuclear spin $I = 5/2$. Each sextet corresponds to the allowed transitions $|M, m\rangle \rightarrow |M - 1, m\rangle$; where M and $m = \pm 5/2, \pm 3/2 \pm 1/2$ are the electron and nuclear spin quantum numbers respectively. Weak doublet lines due to $|1/2, m\rangle \rightarrow |-1/2, m\rangle$ transitions, visible at the centre of the spectrum, are forbidden transitions for which $\Delta M = \pm 1$ and $\Delta m \neq 0$. The spectrum is axially symmetric and can be described by the following spin-Hamiltonian.

$$H = \mu_B[g_{xx}(B_xS_x + B_yS_y) + g_{zz}B_zS_z] + D_{xx}(S_x^2 + S_y^2) + D_{zz}S_z^2 + (1/60)(b_4^0O_4^0 + b_4^3O_4^3) + A_{xx}(S_xI_x + S_yI_y) + A_{zz}S_zI_z.$$

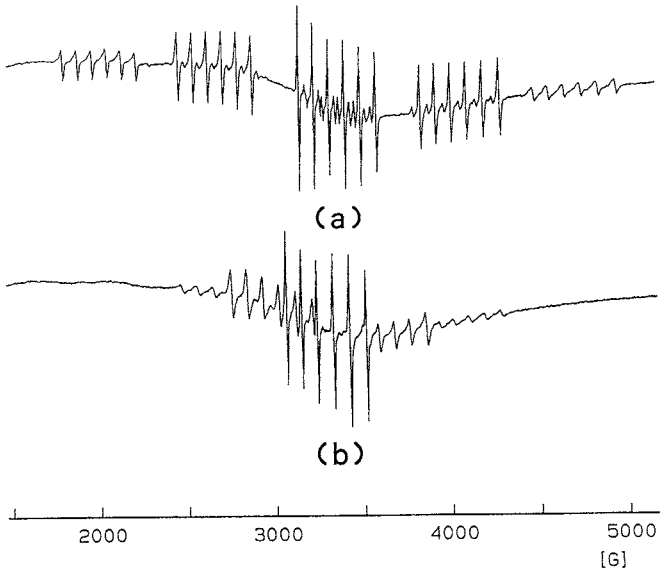

Figure 1. X-band EPR spectrum for KNCr:Mn^{2+} crystal at 291 K for B along the crystallographic c-axis (a) and B in the ab plane (b). The spectrum consists of 30 hyperfine lines due to the electronic spin $S = 5/2$ and nuclear spin $I = 5/2$. Weak doublet lines located in between transitions $|1/2, m\rangle \rightarrow |-1/2, m\rangle$ at the centre of the spectrum, particularly well visible in part (a), are due to forbidden transitions with $\Delta m \neq 0$.

In the above equation, μ_B is the Bohr magneton, O_m^n are spin operators and g_{zz}, g_{xx}, D_{xx}, D_{zz}, b_4^0, b_4^3, A_{zz}, A_{xx} are spin-Hamiltonian parameters [8]. The x-, y- and z-axes coincide with the principal axes of the D tensor. The overall splitting of the spectra is maximum along the z-axis and minimum in the xy plane.

A least-squares fitting procedure utilizing exact numerical diagonalization of the spin-Hamiltonian matrix was carried out using the EPR–NMR computer program [9]. A large number of well-resolved resonant field positions belonging to different sextets and at different orientations of the external magnetic field were used to evaluate spin-Hamiltonian parameters. The agreement between the experimental and calculated magnetic field of resonance lines was excellent for all lines. The spin-Hamiltonian parameters are listed below:

$$g_{xx} = 2.0009 \pm 0.0003,$$
$$g_{zz} = 2.0010 \pm 0.0003,$$
$$D_{xx} = 113.9 \pm 0.4\text{G},$$
$$D_{zz} = -227.8 \pm 0.4\text{G},$$
$$b_4^0 = 0.055 \pm 0.003\text{G},$$
$$b_4^3 = -9.3 \pm 1.7\text{G},$$
$$A_{xx} = 90.9 \pm 0.4\text{G},$$
$$A_{zz} = 89.3 \pm 0.3\text{G}.$$

The values of the zero-field splitting parameters are typical for the octahedral surroundings of the Mn^{2+} ion [10]. This fact indicates that Mn^{2+} is incorporated into the lattice in the position of the Na^+ ion. According to crystallographic data, Na^+ ions are surrounded by an octahedron formed by six oxygens of CrO_4^{2-} anions, all related by symmetry operations in the paraelastic

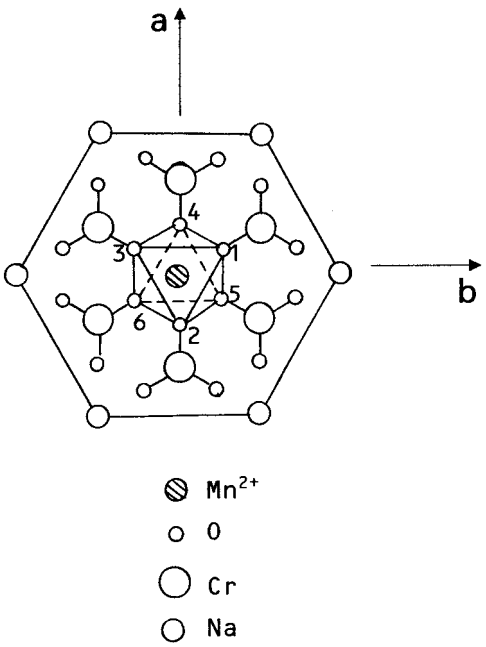

Figure 2. Six oxygen atoms form an octahedron around the Mn^{2+} ion. All atoms are projected onto the *ab* crystallographic plane. Atoms designated 1, 2 and 3 are above the plane containing the Mn^{2+} ion while the remaining atoms are below it. The principal z direction of the zero-field splitting tensor is perpendicular to the two triangles formed by atoms 1, 2, 3 and 4, 5, 6. It is parallel to the three-fold rotation axis of the crystal. Potassium ions designated K(1) are located above and below the Cr ions while potassium ions designated K(2) are located above and below Na ions. The crystallographic data are taken from [3].

phase [3]. The average Na–O distance is 0.2359 nm. The octahedron surrounding the Na^+ ion is shown in figure 2. All atoms are projected onto the *ab* crystallographic plane. Atoms designated 1, 2 and 3 are above the plane containing the Mn^{2+} ion and atoms designated 4, 5 and 6 are below it. The principal direction of the zero-field splitting tensor is perpendicular to two triangular faces of the octahedron, which agrees perfectly with the trigonal distortion of the octahedron.

The size of the Na^+ ion (0.098 nm) is comparable to the size of the Mn^{2+} ion (0.091 nm), which guarantees a minimum distortion of the host lattice. The fact that the univalent Na^+ ion is substituted by the bivalent Mn^{2+} ion means that a charge compensation is required. Often the charge compensation is provided by a nearby vacancy. The best candidate for the vacancy is K^+ ions in the position of K(2). This is located on the three-fold axis (perpendicular to the *ab* plane) in a large cavity formed by 12 oxygen atoms and is the most loosely bound cation in the structure.

Positions of EPR lines due to Mn^{2+} ions are strongly temperature dependent. This dependence can be accounted for by the temperature variation of the zero-field splitting D parameter ($D = 3/2\ D_{zz}$), shown in figure 3, which in turn can be attributed to thermal expansion of the crystal. The following expression was used to describe $D(T)$ dependence in various crystals [11]:

$$D(T) = D(T_0)[1 - 6\gamma(T - T_0)].$$

In the above expression $\gamma = (6.1 \pm 0.2) \times 10^{-5}\ K^{-1}$ is the coefficient of linear thermal

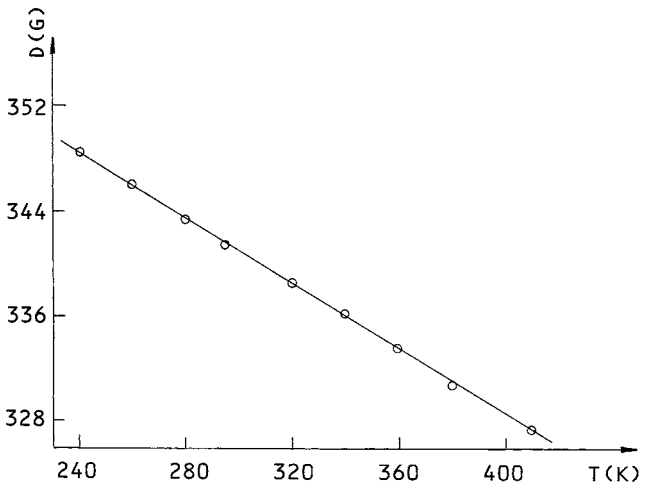

Figure 3. The temperature variation of the zero-field splitting D parameter ($D = 3/2\ D_{zz}$). The change is accounted for by the thermal expansion of the crystal.

expansion and $T_0 = 295$ K is a reference temperature. The linear dependence holds until the phase transition temperature is approached.

4. Phase transformation

A clear signature of the phase transition in the KNCr crystal is the splitting of EPR lines into components. Figure 4 shows the temperature dependence of the lowest magnetic field sextet (transitions $|5/2, m\rangle \rightarrow |3/2, m\rangle$) and two lines of the next lowest-field sextet (transitions $|3/2, m\rangle \rightarrow |1/2, m\rangle$). The spectra were recorded for the magnetic field direction in the bc plane, 6° from the c-axis. The splitting of the lines is initiated at 238 K and is gradual, indicating a continuous (second-order) type of phase transition. This temperature agrees very accurately with the phase transition temperature reported previously [1]. Just below 238 K, the EPR lines exhibit anomalous line shapes characteristic of the existence of an incommensurate phase. A detailed discussion of incommensurability in the KNCr crystal is presented in the next section. At 228 K an additional line splitting is observed. It occurs for all lines but is particularly well resolved for the transitions $|3/2, m\rangle \rightarrow |1/2, m\rangle$. This splitting is gradual and most likely represents the development of the ferroelastic domains. Thus, each EPR line splits into four components: the first splitting occurring at 238 K reflects the doubling of the unit cell while the additional splitting at 228 K reflects the appearance of domains. It is standard notation to designate the phase transition temperature to the incommensurate phase by T_I and the transition temperature from the incommensurate phase to the low-temperature commensurate phase by T_C.

Below the phase transition temperature $T_I = 238$ K, the principal direction of the D tensor is deflected from the c-axis. The rotational diagram for the EPR lines corresponding to the transitions ($|5/2, m\rangle \rightarrow |3/2, m\rangle$) and recorded in the ac plane at 240 K (above T_I) and 208 K (below T_I) is shown in figure 5. The second lowest sextet (transitions $|3/2, m\rangle \rightarrow |1/2, m\rangle$) was found most convenient to study changes occurring at the phase transition. The EPR lines corresponding to transitions $|5/2, m\rangle \rightarrow |3/2, m\rangle$ are quite weak, especially as they are split into four components.

The rotational diagram shown in figure 5 indicates lowering of the crystal symmetry from trigonal to monoclinic. The angle of deflection, designated α, is temperature dependent. The

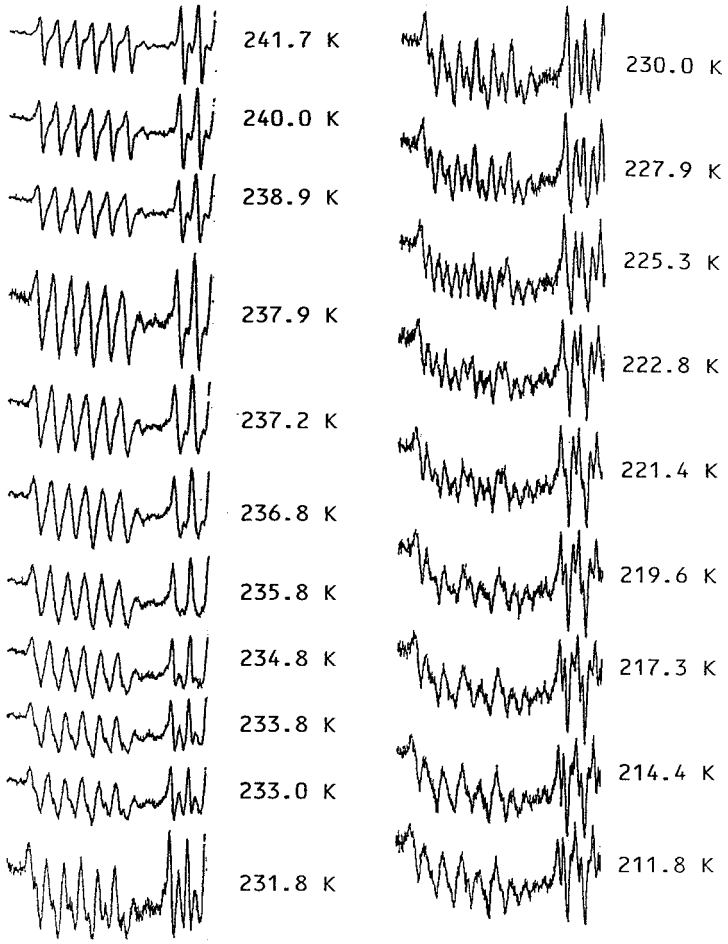

Figure 4. The temperature evolution of the spectrum near the phase transition temperature at 238 K. Only the lowest-field sextet and two lines of the next lowest-field sextet are shown. Just below the phase transition temperature at 238 K, each hyperfine line gives rise to two edge singularities indicating the existence of an incommensurate phase. The edge singularities are initially very asymmetric in terms of the amplitude but become more symmetric as the temperature is lowered. This is particularly well visible for the two lines due to the transitions ($|3/2, m\rangle \rightarrow |1/2, m\rangle$). Below 228 K an additional splitting of lines occurs due to the development of the ferroelastic domains.

angle α varies as $(T_{\mathrm{I}} - T)^{\beta}$, where β is the critical exponent. The log–log graph (figure 6) of the angle α versus $(T_{\mathrm{I}} - T)$ shows that $\beta = 0.48 \pm 0.06$. It is very close in value to the Landau mean-field theory of second-order phase transitions, which predicts $\beta = 0.5$. It is possible that β has a different value in the close vicinity of T_{I}. Unfortunately, reliable measurements of the angle α could not be performed in this temperature range. Surprisingly, the temperature dependence of the angle of deflection observed in the *bc* plane (solid circles in figure 6) is the same as in the *ac* plane (open circles in figure 6). The equality of the angle α in the two planes indicates that the principal z direction of the zero-field splitting tensor is deflected from the c-axis towards the *ab* plane at 45° with respect to the a- and b-axes. Two Mn^{2+} ions, equivalent above the phase transition temperature, become non-equivalent below the phase

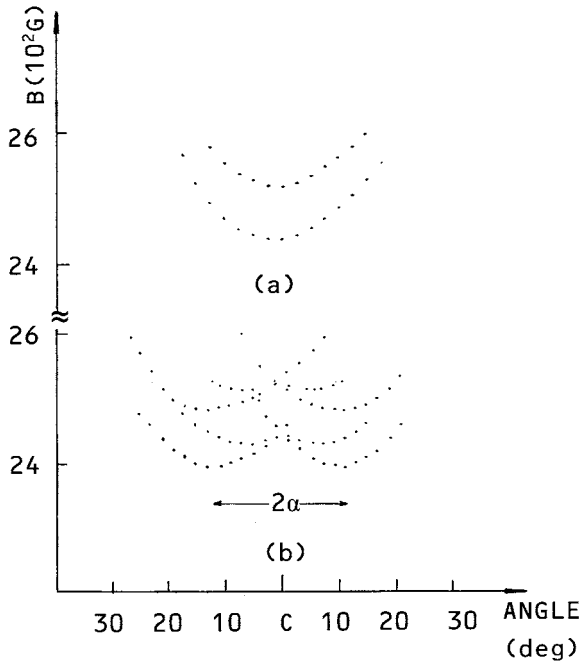

Figure 5. Angular variation of the highest field EPR line in the *ac* plane. Above the phase transition temperature, the maximum coincides with the *c*-axis. This is the principal direction of the zero-field splitting tensor. Below the phase transition at 209 K, the principal direction of the zero-field splitting tensor is deflected by an angle $\alpha = 10.5°$. The same deflection is observed in the *bc* plane.

transition temperature. The increased number of non-equivalent Mn^{2+} ions is related to the doubling of the unit cell. The observed equal deflection of the principal magnetic z-axis in the *ac* and *bc* planes could be due to the shift of the oxygens along the *c*-axis. According to the crystallographic data [3], atomic displacements are accompanied by a gradually increasing shift and tilt of the CrO_4^{2-} anions. Precise correlation of the reported displacements of oxygens around the Mn^{2+} ions with the deflection of the principal magnetic z-axis is very difficult to accomplish.

The deflection of the principal magnetic z-axis at 45° with respect to the a- and b-axes might be related to the previously reported lack of anisotropy of the thermal expansion and dielectric constant along the a and b crystallographic axes below the temperature T_I [1]. This is quite unusual for a crystal with monoclinic symmetry. It is explained by the existence of uniformly distributed ferroelastic domains.

5. Incommensurate phase

The EPR lines are very asymmetric below $T_I = 238$ K with a line shape characteristic of the existence of an incommensurate phase. Two so-called edge singularities are clearly visible in figure 4 for all lines but particularly so for the transitions $|3/2, m\rangle \rightarrow |1/2, m\rangle$. A few additional line shapes are shown in figure 7 for different orientations of the crystal with respect to the magnetic field and at various temperatures. The intensity of the two singularities is very different and changes with temperature. The occurrence of the edge singularities is explained

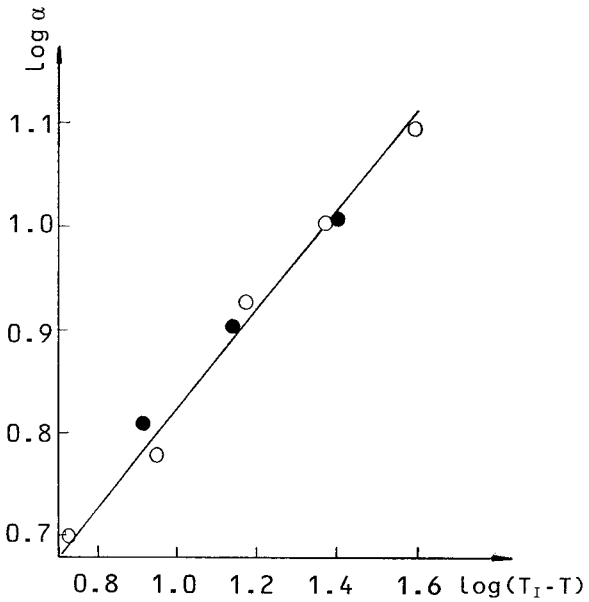

Figure 6. A log–log graph of the angle of deflection α of the principal direction of the zero-field splitting tensor from the c-axis versus the difference of temperature from 238 K. The open circles represent the angle α measured in the ac plane while solid circles represent the angle α measured in the bc plane. The change of the angle α is gradual and indicates a second-order type phase transition. Close to the phase transition the lines were too weak and too asymmetric to determine the angle α accurately.

in the following way. For static spatial modulation in one dimension (along the z-axis) and in the so-called plane wave limit, the lattice displacements $u(z)$ are described in a simple form:

$$u(z) = A(z)\cos[\Phi(z)].$$

$A(z)$ is the amplitude and the phase $\Phi(z) = q_{\mathrm{I}}z + \Phi_0$, where q_{I} is the incommensurate wavevector [12].

The resonance magnetic field B_{r} is a function of lattice displacements and its deviation from the resonance field B_0 observed in the absence of modulation can be written as a power series:

$$\Delta B = B_{\mathrm{r}} - B_0 = h_1 A(z)\cos[\Phi(z)] + h_2[A(z)]^2\cos^2[\Phi(z)] + \cdots.$$

Two additional parameters introduced in the above equation, h_1 and h_2, depend on the field B. The linear term for the KNCr crystal is forbidden due to the symmetry elements of the paraelastic phase. The paramagnetic sites corresponding to the condition $\mathrm{d}[\Delta B(\Phi)]/\mathrm{d}z = 0$ give rise to two singularities superimposed on a continuous absorption line. The two edge singularities are not necessarily of equal intensity.

In the incommensurate phase the number of non-equivalent Mn^{2+} sites is infinite. The experimental line shape is the sum of the local lines.

$$F(B - B_{\mathrm{r}}) = \int f[(B - B_{\mathrm{r}} + \Delta B)/L]\,\mathrm{d}\Phi.$$

The integration is over all values of the phase angle, f is the general line shape (Lorentzian or Gaussian) and L is the width of the line [12].

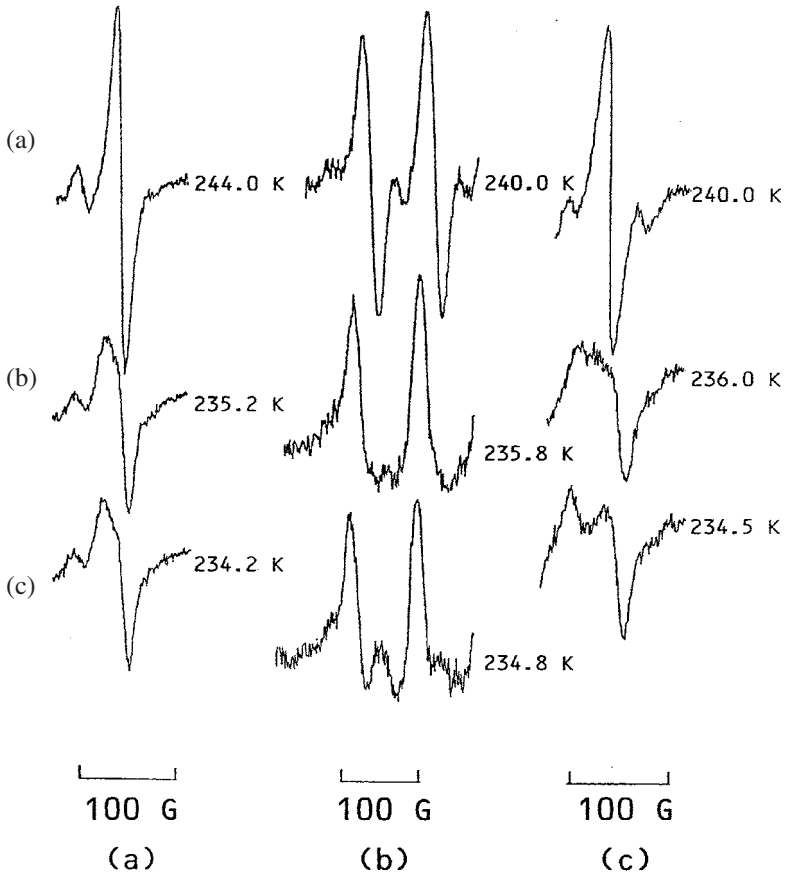

Figure 7. A few examples of line shapes recorded for KNCr:Mn^{2+} crystal for various crystal orientations and at various temperatures. (a) Highest-field $|3/2, m\rangle \rightarrow |1/2, m\rangle$ hyperfine transition for the magnetic field B direction 2° from the c-axis in the ac plane. (b) Two lowest-field $|3/2, m\rangle \rightarrow |1/2, m\rangle$ hyperfine lines recorded for a B direction 6° from the c-axis in the bc plane. (c) Highest-field $|3/2, m\rangle \rightarrow |1/2, m\rangle$ hyperfine transition for the magnetic field B direction 10° from the c-axis in the ac plane. Two edge singularities are observed below the phase transition temperature. Their amplitude and separation are temperature dependent.

As the temperature decreases, the two singularities become more symmetric, indicating gradual transformation of the incommensurate phase from the plane wave regime into the soliton regime. In this regime the phase $\Phi(z)$ becomes a nonlinear function of z and is described by the sine–Gordon equation. Solitons develop and their width and density change with decreasing temperature. The temperature at which the wavevector q_I locks into a commensurate value corresponds to a phase transition to a low-temperature (ferroelastic) commensurate phase. This temperature is most likely signified by the additional splitting of lines observed at 228 K. It correlates quite well with the phase transition temperature $T_C = 231$ K reported based on Brillouin scattering measurements [2].

Various simulated EPR line shapes are described in the plane wave and soliton regimes [12–16]. A model in which both linear and quadratic local line shifts are included [16], the broad soliton model [14] and incommensurate modulation with variation of the spin–lattice relaxation rate over the spectrum [15] lead to very asymmetrical singularities.

An additional factor contributing to the intensity difference of the two singularities might be that they correspond to different angles α on the rotational diagram. The singularity on the large slope on the rotational diagram is weak while the singularity corresponding to the 'flat' dependence of ΔB on the angle α might be stronger. However, for all orientations of the crystal, even for the magnetic field B parallel to the c-axis, lines just below $T_I = 238$ K are very asymmetric.

The existence of an incommensurate phase is not the only way to account for the asymmetry of EPR lines showing edge singularities. For example, asymmetrical EPR lines with two edge singularities observed in $MgSiF_6{\cdot}H_2O{:}Mn^{2+}$ have been explained in terms of the existence of broad antiphase domain walls [17]. However, in a similar crystal, $MgGeF_6{\cdot}H_2O{:}Mn^{2+}$, this model was not as successful in fitting the EPR line shapes as when using the modulated crystal structure [15].

Another possible way to account for the asymmetry of the EPR lines might be the presence of statistical disorder of the trigonal deformation of the octahedron surrounding Mn^{2+}. Statistical distribution of the angle α due to various crystal imperfections could cause asymmetric lines. However, it is not clear if two edge singularities of different amplitude can be associated with statistical disorder.

Two phenomenological models of the phase transition in KNCr have been proposed. One of the models [2] was constructed based on the point symmetry change from $\overline{3}m$ to $2/m$. This symmetry change was attributed to the Γ point ($\mathbf{K} = 0$) two-dimensional representation E_g. Terms cubic in the order parameter were incorporated in the free-energy expansion. This helped to account for the weak first-order character of the phase transition and possibility of the existence of a metastable phase. A second model [6] was proposed based on the knowledge that the space group changes from $P\overline{3}m1$ to $C2/c$ with the doubling of the unit cell. The reduction of symmetry requires a representation with $\mathbf{K} \neq 0$. The space group symmetry change can be explained by a two-dimensional irreducible representation A_3^+ at the A point of the first Brillouin zone ($\mathbf{K} = \mathbf{g}_1/2$). The incommensurate phase exists if the thermodynamic potentials have minima that lie not at the symmetric point of the Brillouin zone, such as point A, but rather in general positions in the vicinity of point A. The thermodynamic potential used in [6] should include terms allowed by symmetry of the crystal such as a Lifshitz invariant

$$a(Q_1\,\mathrm{d}Q_2/\mathrm{d}z - Q_2\,\mathrm{d}Q_1/\mathrm{d}z)$$

or squared gradient invariant

$$b_1(\mathrm{d}Q_1/\mathrm{d}z)^2 + b_2(\mathrm{d}Q_2/\mathrm{d}z)^2.$$

In the above expressions, Q_1 and Q_2 are two components of the order parameter and a, b_1 and b_2 are constants. The inclusion of these terms in the thermodynamic potential prevents the direct transition from the paraelastic phase into the commensurate ferroelastic phase [18].

The presence of the incommensurate phase in the KNCr crystal needs to be confirmed by other experimental techniques, such as x-ray diffraction. Observation of satellite reflections would confirm its existence. Detailed x-ray diffraction measurements were conducted in the KNCr crystal at $T = 200$ K, approximately 39 K below the phase transition. No satellite reflections have been reported. This is not surprising because the EPR lines at 200 K are symmetric, indicating that the phase is commensurate at this temperature. However, it was observed that the amplitudes of some x-ray reflections increase dramatically below the phase transition [3].

Small anomalies of the dielectric constant ε'' were detected in the transition region [1]. These anomalies were not repeatable but could indicate some processes associated with the existence of the incommensurate phase.

Two crystals, KNSe and KNCr, show a number of similarities. They are isostructural in the paraelastic phase and undergo identical changes in space group symmetry at the phase transition. In both crystals the mechanism of the phase transition seems to be related to the shift of K(2) ions and the tilt of tetrahedral groups. The main difference between the two crystals is the existence of an intermediate phase in the KNSe crystal, separated by two phase transitions at 346 and 329 K. It is likely that the intermediate phase observed in the KNSe is an incommensurate phase.

6. Conclusions

Spin-Hamiltonian parameters for the Mn^{2+} ion in KNCr crystal were determined. The Mn^{2+} ions substitute for Na^+ and are surrounded by an octahedron formed by six oxygens of CrO_4^{2-} anions. The principal direction of the fine structure tensor is along the crystallographic *c*-axis (three-fold axis). The paramagnetic centre is isotropic in the *ab* crystallographic plane.

The phase transformation into the ferroelastic state occurs through an incommensurate phase. Its existence has been deduced by observation of very asymmetric the EPR lines showing two edge singularities. The phase transition to the incommensurate phase at $T_I = 238$ K is of the second-order type as indicated by a gradual splitting of EPR lines. The lock-in transition to the commensurate ferroelastic phase may occur at 228 K, signified by an additional splitting of lines.

The principal direction of the zero-field splitting tensor, which is along the three-fold *c*-axis above T_I, is deflected 12° at 202 K in both the *ac* and *bc* crystallographic planes. This deflection is related to the rearrangement of the atoms leading to the doubling of the unit cell. The shift of the oxygen atoms along the *c*-axis could account for this change. This could be accomplished by an appropriate tilt of the CrO_4 groups.

Irradiation of pure KNCr crystals with gamma rays does not lead to the creation of CrO_4 radicals due to their fast recombination. Substitution of CrO_4 by SeO_4 groups and subsequent irradiation of crystals produced SeO_4^{3-} and SeO_3^- radicals. Only radicals corresponding to Se with nuclear spin $I = 0$ were strong enough to be detected, while radicals corresponding to Se isotopes with $I = 1/2$ were too weak to be observed.

Acknowledgment

I am very grateful to Professor J M Boggs for use of the EPR spectrometer.

References

[1] Krajewski T, Mroz B, Piskunowicz P and Breczewski T 1990 *Ferroelectrics* **106** 225
[2] Mroz B, Kiefte H, Clouter M J and Tuszynski J A 1991 *Phys. Rev.* B **43** 641
[3] Fabry J, Breczewski T and Madariaga G 1994 *Acta Crystallogr.* B **50** 13
[4] Fabry J, Petricek V, Vanek P and Cisarova I 1997 *Acta Crystallogr.* B **53** 596
[5] Mroz B, Kiefte H, Clouter M J and Tuszynski J A 1992 *Phys. Rev.* B **46** 8717
[6] Diaz-Hernandez J, Manes J L, Tello M J, Lopez-Echarri A, Breczewski T and Ruiz-Larrea I 1996 *Phys. Rev.* B **53** 14097
[7] Jerzak S and Mroz B 2002 *J. Phys.: Condens. Matter* **14** 8121
[8] Abragam A and Bleaney B 1979 *Electron Paramagnetic Resonance of Transition Ions* (Oxford: Clarendon) pp 139–42
[9] Weil J A *Computer Program EPR–NMR* Department of Chemistry, University of Saskatchewan, Canada
[10] Misra S K and Jerzak S 1989 *Phys. Rev.* B **39** 2041
[11] Misra S K and Kahrizi M 1985 *J. Chem. Phys.* **83** 1490
[12] Muller K A and Thomas M 1981 *Structural Phase Transitions* vol 2 (Berlin: Springer) pp 62–4

[13] Fujimoto M 1997 *The Physics of Structural Phase Transitions* (Berlin: Springer) pp 211–27
[14] Blinc R 1981 *Phys. Rep.* **79** 331
[15] Skrylnik P G and Ziatdinov A M 2002 *J. Phys.: Condens. Matter* **14** 11671
[16] Emery J, Hubert S and Fayet J C 1985 *J. Physique* **46** 2099
[17] Zapart W and Zapart M B 1999 *Bull. Magn. Reson.* **19** 34
[18] Toledano J C and Toledano P 1987 *The Landau Theory of Phase Transitions* (Singapore: World Scientific) pp 215–95